Clipping-Free Multilayer Optical OFDM for IM/DD-based Communication Systems

Hongxu Wang, Huixin Zhang, Zabih Ghassemlooy and Tian Zhang*

***Abstract*—A low-complexity and high-performance clipping-free multilayer optical orthogonal frequency division multiplexing scheme is proposed for optical wireless communication (OWC). At the transmitter, the symbols of multi-layer quadrature amplitude modulation (QAM) are first arranged according to a specific rule in the frequency domain to generate a bipolar time-domain signal using a single inverse fast Fourier transform (IFFT). Then the bipolar signal is superimposed with an adaptive periodic DC bias to meet the real and positive requirements in intensity modulation / direct detection (IM/DD) systems. At the receiver, a zero-value regression (Re0) -based demodulation is proposed to optimize the bit error rate (BER). As the signal generation and demodulation are realized by single IFFT and fast Fourier transform (FFT) respectively, the proposed scheme has nearly the same system complexity as the single-layer modulations and similar spectral efficiency with those advanced multilayer modulations. In addition, the proposed periodic DC improves the power efficiency and avoids the interlayer interference. Numerical simulation results show that, compared with LACO-OFDM [34] with 3 layers, the proposed scheme can attain a PAPR gain of 2.4 dB and BER gain of 1.4 dB and 3 dB for the linear and nonlinear channel, respectively.**

***Index Terms*—Optical wireless communication, Complexity, Spectral efficiency, Bit error rate, Peak-to-average power ratio.**

I. INTRODUCTION

THE information age with the requirements for high volume data, higher speed, and lower latency poses new challenges to the existing communications networks. In addition, in intelligent-based communication networks the data mining and processing of ever-growing massive data is introducing further challenges to the service providers. Therefore, in recent years we have seen growing research activities in virtual reality (VR), deep learning technology (including artificial intelligence (AI)), and deep learning-based communication technologies, which are showing immense potential in communication networks, modulation/coding identification, channel estimation, signal detection and processing [1]. Thus, leading to more efficient, stable, reliable and low-latency connection modes (i.e., access points).

Manuscript received XXXX XX, 2022. This work was supported in part by the scientific research Project of Education Department of Jilin Province under Grant JJKH20231294KJ, in part by the National Natural Science Foundation of China under Grant 11905028, and in part by the Foundation for Excellent Young Talents of Jilin Province under Grant 20190103010JH. The associate editor coordinating the review of this article and approving it for publication was XXXXX. (Corresponding author*: Tian Zhang).

Hongxu Wang, Huixin Zhang and Tian Zhang are with the School of Physics, Northeast Normal University, Changchun 130024, China (e-mail: zhangt100@nenu.edu.cn).

Zabih Ghassemlooy is with the Optical Communications Research Group, Faculty of Engineering and Environment, Northumbria University, Newcastle upon Tyne NE1 8ST, U.K.

The radio frequency (RF)-based communication network has served very well to meet the user requirements for decades. However, with the exponential growth in data being generated there is a need to look for other complementary wireless solutions that will ease the pressure on the RF systems. Therefore, within this context, moving to the higher carrier frequencies of millimeter-wave, tera Hertz, and optical would be a logical option, which facilitates the use of multiple (i.e., hybrid) wireless technologies as part of fifth- and sixth-generation wireless networks.

In the optical domain, the visible light communication (VLC) as part of optical wireless communication (OWC) is seen as a potential wireless technology that could be used in applications where RF systems are not the desired option [2]. VLC as a green wireless technology offers advantages such as security, lower energy usage, a wide range of data rates up to a few Gbps over a short-range transmission using light emitting diode (LED)-based light access points (i.e., no need for additional RF access points), no electromagnetic interference, etc. [3-5]. In addition, VLC networks can be implemented using power line communications or power of ethernet cables. Note, the latter eliminates the expense of installing additional electrical wiring, which can send 10/100/1000 Mbps of data and 15/30/60/90 W of power, which is more than sufficient for LED lighting, over a maximum distance of 100 m. In addition, VLC can be combined with WiFi to ensure link availability in indoor environments as part of the realization of sixth-generation wireless communication networks [6], [7].

The simplicity of the VLC technology lies in the intensity modulation/direct detection (IM/DD) scheme, which uses LEDs and photodiodes (PDs) as the transmitter (Tx) and receiver (Rx), respectively. In IM/DD VLC systems we note the following: (i) the signal is usually one-dimensional and unipolar; (ii) LED modulation bandwidth B_{LED}, which determines the volume of information that can be transmitted; (iii) LED linearity, which is critical in multi-carrier and multi-level modulation schemes to ensure high peak-to-average power ratio (PAPR), as well as; and (iv) dimming i.e., operation at low illumination levels without effecting data transmission [2], [8], [9].

As for increasing the data rates, there are several options including LEDs with higher B_{LED}, equalization, wavelength division multiplexing (WDM) and multi-carrier modulations such as orthogonal frequency division multiplexing (OFDM) [2], [10], [11]. Combined with the relevant technical requirements of VLC, the optical OFDM (O-OFDM) has been extensively studied in OWC including VLC [12]. In OFDM the one-dimensional requirement is realized by inverse fast

Fourier transform (IFFT) with Hermite symmetric distribution of the quadrature amplitude modulation (QAM) symbol or the pulse amplitude modulated (PAM) symbol. For the generated bipolar real signal, some additional operations are required to realize its unipolarity, e.g., DC-biased O-OFDM (DCO-OFDM) [13]. However, this way of adding the DC bias will result in lower power efficiency (PE), and down clipping will further deteriorate the bit error rate (BER) performance of the system. Compared with the DCO-OFDM, asymmetrically clipped O-OFDM (ACO-OFDM) and pulse amplitude modulated discrete multitone (PAM-DMT) use special frequency-domain structures to introduce negative clipping without the loss of any information and meet the unipolar requirements of the output signal [14], [15]. However, this results in not utilizing the even carriers and the real part of the carrier, respectively, thus leading to lower spectral efficiency (SE), which is not desirable in highspeed VLC links.

To improve both PE and SE in OWC, hybrid/layered modulation schemes have been proposed to explore the wasted blank carriers [16-19]. In [20], a hybrid ACO-OFDM (HACO-OFDM), based on ACO-OFDM, was investigated, where the imaginary part of even carriers was used to load PAM symbols to improve the SE on the premise of maintaining the system PE. However, this improvement is gained at the cost of (i) increased IFFT because of the layered modulation at the Tx; (ii) a complex Rx; and (iii) BER deterioration due to the interlayer interference. In [21], layered ACO-OFDM (LACO-OFDM) was proposed with the SE limit approaching that of DCO-OFDM by means of the superposition of multi-layer ACO-OFDM. Although LACO-OFDM offers higher SE than HACO-OFDM the system complexity increases with the number of layers i.e., the layered signal generation and iterative demodulation. Both HACO-OFDM and LACO-OFDM suffer from interlayer interference, which leads to the deterioration of the BER performance. Thus, the trade-off between SE, PE, complexity, and performance is important in OWC [22], [23]. In short, a system with excellent performance should not only have higher SE and PE, but also have lower BER and less complex transceivers [24], [25]. In this context, several balanced modulation and demodulation schemes based on conventional ACO-OFDM, DCO-OFDM and PAM-DMT have been proposed recently in the literature. In addition, HACO-OFDM, LACO-OFDM, asymmetrically clipped DC-biased O-OFDM (ADO-OFDM), and PAM-DMT-based hybrid Optical OFDM (PHO-OFDM) are introduced [26-29]. Pairwise averaging (PA), pairwise clipping (PC), and other optimization techniques have been proposed to mitigate interlayer interference at the cost of increased system complexity.

A low-complex Rx was proposed for HACO-OFDM OWC by distinguishing the two-layer signal in the time domain with a branch PC operation [30]. Furthermore, another interference-free hybrid O-OFDM (IFHO-OFDM), which is less complex, was reported in [32], which used a small DC bias value at the Tx to remove the negative clipping in ACO-OFDM. Considering that, in this scheme there is no interlayer interference, therefore the Rx can be further simplified by a single fast Fourier transform (FFT)-based demodulation scheme. It offers similar BER and SE compared to conventional HACO-OFDM. The use of a single FFT-based Rx in LACO-OFDM has resulted in reduced system complexity [33], [34]. However, the Tx complexity still needs addressing.

In this paper, a zero-value regression (Re0) based clipping-free multilayer O-OFDM (CFMO-OFDM) scheme is proposed for optical wireless communications. In this scheme, multi-layer ACO-OFDM signals are superimposed in the time domain with no clipping, and a periodic adaptive DC bias is used to ensure unipolarity of the signal for intensity modulation of the optical light source. Note that, (i) due to the special periodicity of DC bias, the generated noise will all fall on the unused subcarriers in the frequency domain, thus not affecting the information data; (ii) with no negative clipping signal generation can be realized using single-IFFT at the Tx instead of generating the signals of each layer separately; and (iii) realization of signal demodulation and data recovery by employing only single-FFT at the Rx. As for the Re0 algorithm, the inherent zero value generated by the addition of adaptive DC bias is forcibly zeroed to remove the noise of corresponding carrier signals in the time domain. Note, the number of cycles of the adaptive DC bias increases with the stacking layers, thus leading to the decreasing inherent zero value of the system and the reduced denoising effect.

The advantages of this scheme are briefly introduced as follows:

1) In terms of SE [35], [36], the proposed scheme can achieve similar performance to LACO-OFDM and can approach the limit of DCO-OFDM.
2) In terms of complexity, the number of FFT/IFFT used by the proposed scheme at the Tx and the Rx is like that of a single-layer modulation/demodulation scheme [37].
3) In terms of PE, the level of the added adaptive DC bias is very small, which is much smaller than that of DCO-OFDM [38], [39]. Since the proposed scheme does not suffer from interlayer interference and down-clipping distortion, the small power efficiency loss caused by the adaptive DC bias can be compensated from the perspective of system BER [40].
4) In terms of the peak-to-average power ratio (PAPR), the proposed scheme only applies high DC bias to extreme signals rather than all signals, which makes the PAPR of the proposed scheme lower than LACO-OFDM and HACO-OFDM for example. Thus, showing high tolerance to the LED nonlinearity [41], [42].
5) In terms of BER, the numerical simulation results show that the proposed scheme offers improved performance compared with DCO-OFDM, HACO-OFDM, LACO-OFDM, and other schemes reported in the literature [13], [20] and [21] under the same SE.

The contents of this paper are organized as follows: the introduction of CFMO-OFDM with the Tx and Re0 Rx is given in Section II. The BER, complexity, SE, and PAPR performance of the proposed scheme are analyzed in Section III. The comprehensive numerical simulations including the coding algorithm, Re0 Rx, linear and nonlinear channel, and a proof-of-concept experiment are given in Section IV. Finally, the conclusion of this paper is given in Section V.

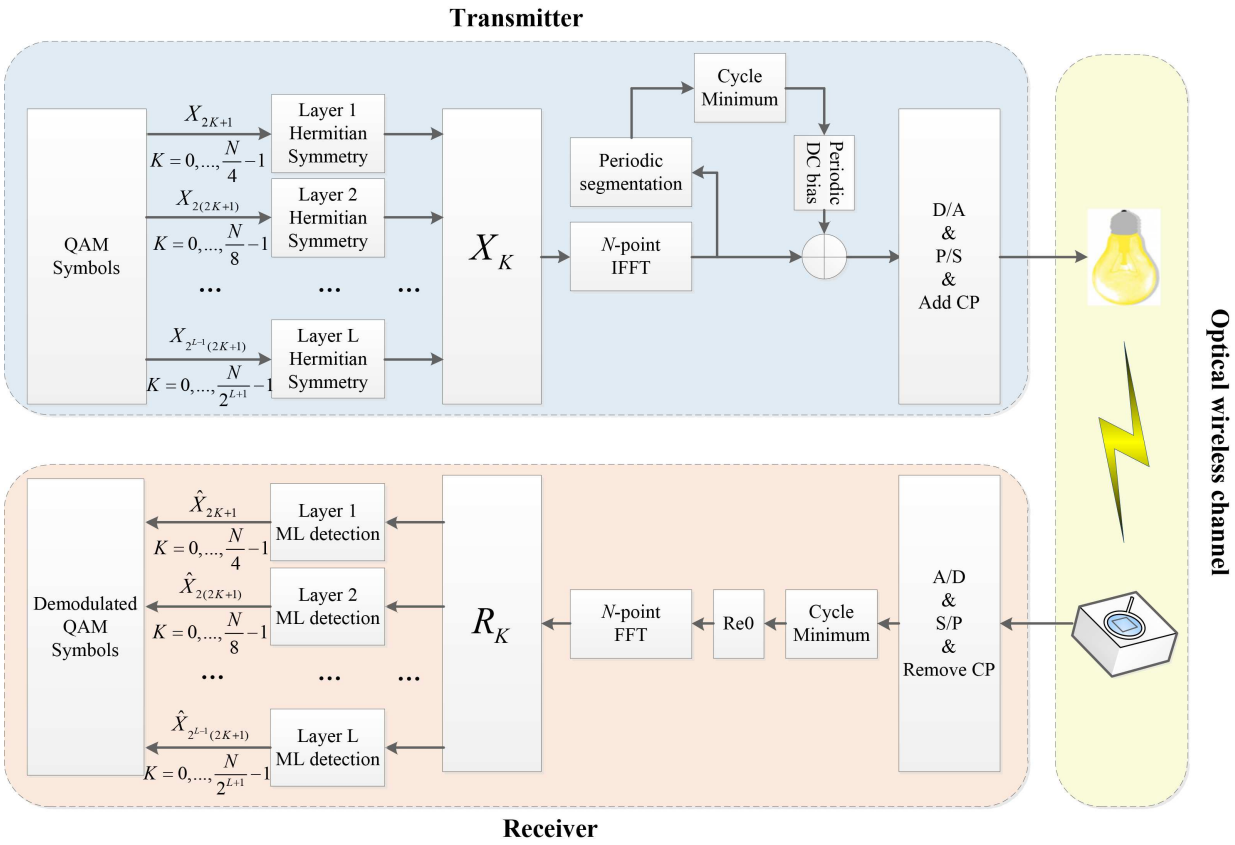

Fig. 1: Block diagram of the proposed CFMO-OFDM scheme with Re0 receiver.

II. Proposed CFMO-OFDM

This section introduces the CFMO-OFDM scheme for an IM/DD-based OWC link in detail. Firstly, the CFMO-OFDM transmitter is introduced. Then, the principle of adaptive periodic DC bias is given. Finally, we analyze the inherent zero value of the time-domain signal and introduce the Re0 Rx for the CFMO-OFDM system.

A. CFMO-OFDM Transmiter

For L-layer CFMO-OFDM scheme with N subcarriers ($1 \leq L \leq \log_2 N - 1$), in the frequency domain $\{X_{2^{l-1}(2K+1)}, (0 \leq K \leq \frac{N}{2^l} - 1)\}$ of subcarrier is occupied by the l-th layer ACO-OFDM ($1 \leq l \leq L$) with QAM symbol, thus leaving with the unused subcarriers of $\{X_{K \cdot 2^L}, (0 \leq K \leq \frac{N}{2^L} - 1)\}$. At the same time, Hermite symmetry is applied to ensure the real value of the generated time domain signal. Note, for (i) $L = 1$, the SE is consistent with that of ACO-OFDM; and (ii) $L = \log_2 N - 1$, only the 0-th and the $N/2$-th subcarriers are unoccupied, therefore the SE is in line with DCO-OFDM. The symbol modulation in the frequency domain is as follows:

$$X = [X^l_{2^{l-1}(2K+1)}, (X^l_{2^{l-1}(2K+1)})^*], \quad 1 \leq l \leq L,\ 0 \leq K \leq \frac{N}{2^{l+1}} - 1. \tag{1}$$

where $(\cdot)^*$ represents the conjugate operation. $X^l_{(\cdot)}$ represents the mapping symbol of the l-th layer.

Note that the modulated symbols of all layers in (1) are fed into the same IFFT module at the same time, rather than being generated separately as adopted in other hybrid modulation schemes. Therefore, the time-domain bipolar output signal can be given by:

$$x_n = \frac{1}{\sqrt{N}} \sum_{K=0}^{N-1} X_K \exp(j \frac{2\pi}{N} nK). \tag{2}$$

However, in (2) cannot be used for direct transmission, and therefore needs DC biasing to generate a unipolar signal. The adaptive periodic DC bias is proposed and introduced here. First, the time-domain signal obtained in (2) is divided into 2^L parts by the periodic division operation. The length of each part is equal and determined by the number of layers L initially set by CFMO-OFDM. Then, each part has $\frac{N}{2^L}$ samples. For visualization, we can introduce a $2^L \times \frac{N}{2^L}$ matrix x_M to describe:

$$x\_M = \begin{bmatrix} x_{0+0\times\frac{N}{2^L}} & x_{1+0\times\frac{N}{2^L}} & \cdots & x_{\frac{N}{2^L}+0\times\frac{N}{2^L}-1} \\ x_{0+1\times\frac{N}{2^L}} & x_{1+1\times\frac{N}{2^L}} & \cdots & x_{\frac{N}{2^L}+1\times\frac{N}{2^L}-1} \\ \cdots & \cdots & \cdots & \cdots \\ x_{0+(2^L-1)\times\frac{N}{2^L}} & x_{1+(2^L-1)\times\frac{N}{2^L}} & \cdots & x_{\frac{N}{2^L}+(2^L-1)\times\frac{N}{2^L}-1} \end{bmatrix}. \tag{3}$$

In (3), each row represents a part of x_n after periodic dividing. Then take the minimum value of each part, that is, the minimum value of each column in (3), a $1 \times \frac{N}{2^L}$ row vector will be obtained. Next, we reverse the sign of the vector and

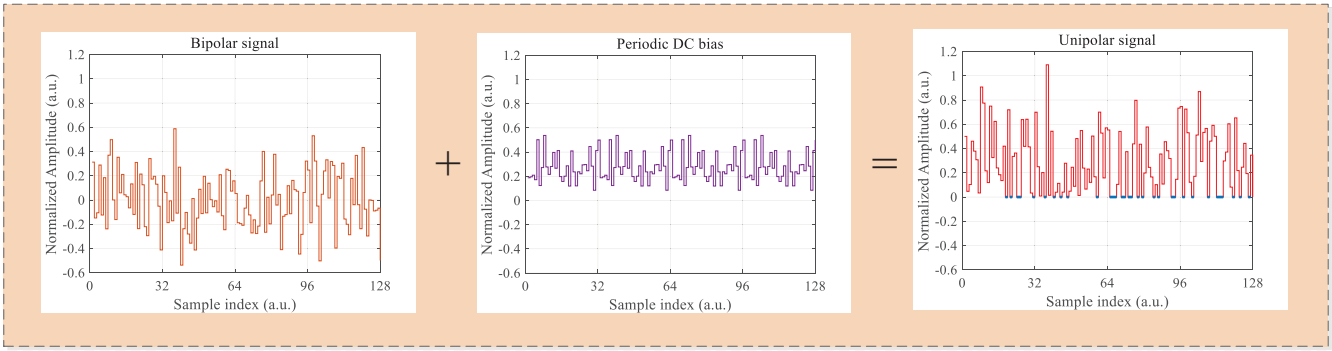

Fig. 2: The time-domain CFMO-OFDM signal with 128 subcarriers and 2 Layers.

define it as a cycle of the added DC bias, which is given by:

$$dc_n = -\min(x\_M, \text{column}). \tag{4}$$

where $\min(A, \text{column})$ represents the operation of minimizing all columns of the matrix A, i.e., cycle minimum (CM) operation. Then the row vector dc is repeated 2^L times to obtain the required DC bias as given by:

$$x\_dc_n = \underbrace{[dc_n, dc_n, ..., dc_n]}_{\text{Repeat } 2^L \text{ Times}}. \tag{5}$$

By superimposing the time-domain signal x_n generated in equation (2) with the DC bias x_dc_n obtained in equation (5), the unipolar time-domain signal t_n can be obtained:

$$t_n = x_n + x\_dc_n. \tag{6}$$

The DC bias level is defined as follows:

$$\beta = 10\log_{10}(1 + \frac{E\left\{x\_dc_n^2\right\}}{\sigma^2_{\text{CFMO}}})(\text{dB}). \tag{7}$$

where σ_{CFMO} represents the root mean square of the CFMO-OFDM bipolar signal.

Table I shows the added DC bias values for different layers and QAM constellation orders (i.e., $N = 512$). Note, for each layer the required DC bias level remains unchanged for each order of QAM. Compared with the classical DCO-OFDM respectively requiring 7, 9, and 10 dB of DC bias values for 16-, 64-, and 256-QAM [39], the proposed adaptive DC bias can further improve the power efficiency of CFMO-OFDM. And it is worth noting that, even at a large DC bias level, DCO-OFDM is still affected by down clipping during the transmission process. Note, in CFMO-OFDM the DC bias level increases with the number of layers. However, when the number of layers is high enough, further increasing the number of stacking layers does not bring great improvement in the SE.

Fig. 2 shows the time-domain CFMO-OFDM signal, in which the number of modulation layers L is set to 2. In order to show the distribution characteristics more clearly in the time domain, we have adopted $N = 128$.

For the added adaptive DC bias, because it has 2^L period in one frame, it will not fall on the $X_{K\cdot 2^L+m}$ $(0 \le K \le \frac{N}{2^L} - 1, 1 \le K \le 2^L - 1)$ subcarrier in the frequency domain, that is, the data subcarriers. Therefore, the adding process of adaptive DC bias will not affect the data transmission. The principle is proved as follows:

$$\begin{aligned} DC_K &= \frac{1}{\sqrt{N}} \sum_{n=0}^{N-1} x\_dc_n \exp(-j\frac{2\pi}{N} nK) \\ &= \frac{1}{\sqrt{N}} \sum_{n=0}^{\frac{N}{2^L}-1} \sum_{\tau=0}^{2^L-1} x\_dc_n \exp(-j\frac{2\pi}{N}(n + \tau\frac{N}{2^L})K). \\ &0 \le K \le N-1 \end{aligned} \tag{8}$$

where DC_K is the frequency-domain signal of x_dc with FFT. The numerical derivation of $DC_{K\cdot 2^L+m}(0 \le K \le \frac{N}{2^L}-1, 1 \le m \le 2^L - 1)$ is given below:

$$\begin{aligned} DC_{K\cdot 2^L+m} &= \frac{1}{\sqrt{N}} \sum_{n=0}^{\frac{N}{2^L}-1} x\_dc_n \exp(-j\frac{2\pi}{N} n(K\cdot 2^L + m))\cdot \\ &\quad \sum_{\tau=0}^{2^L-1} \exp(-j2\pi\tau\frac{(K\cdot 2^L+m)}{2^L}) \\ &= \frac{1}{\sqrt{N}} \sum_{n=0}^{\frac{N}{2^L}-1} x\_dc_n \exp(-j\frac{2\pi}{N} n(K\cdot 2^L + m))\cdot \\ &\quad \sum_{\tau=0}^{2^L-1} \exp(-j2\pi\tau\frac{m}{2^L}) \\ &= \frac{1}{\sqrt{N}} \sum_{n=0}^{\frac{N}{2^L}-1} x\_dc_n \exp(-j\frac{2\pi}{N} n(K\cdot 2^L + m))\cdot \\ &\quad \frac{1-\exp(-j2\pi m)}{1-\exp(-j2\pi\frac{m}{2^L})} = 0 \\ &\quad 0 \le K \le \frac{N}{2^L} - 1, 1 \le m \le 2^L - 1. \end{aligned} \tag{9}$$

Through the proof of (9), it can be seen that the adaptive DC bias is zero on data subcarriers. Fig. 3 shows the frequency-domain characteristics of CFMO-OFDM. For the convenience of observation and description, we set the parameters as $L = 2$ and $N = 16$. It can be seen that the data subcarriers and adaptive DC bias occupy their corresponding carriers without

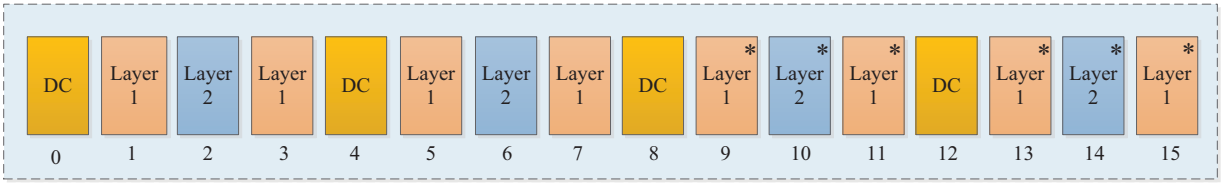

Fig. 3: The frequecy-domain characteristics of CFMO-OFDM with 16 subcarriers and 2 Layers.

mutual interference.

After digital to analog (D/A) conversion, parallel to serial (P/S) conversion and adding cyclic prefix (CP), the generated CFMO-OFDM signal can be transmitted through the light source of LED over the optical wireless channel as shown in Fig. 1.

TABLE I: DC bias level under different layers and QAM order.

Layer	QAM order	DC Bias level (dB)
2	4, 16, 64, and 256	4.36
3	4, 16, 64, and 256	5.55
4	4, 16, 64, and 256	6.59
5	4, 16, 64, and 256	7.50

B. Re0 Reciever

At the Rx, the regenerated electrical signal is given by:

$$r_n = t_n \otimes h_n + w_n. \tag{10}$$

where w_n and h_n denote the discrete additive white Gaussian noise (AWGN) and the channel impulse response (CIR), respectively [43-45]. After receiving the transmitted signal, analog to digital (A/D) conversion, serial to parallel (S/P) conversion and CP removal are still needed.

From the CFMO-OFDM signal generation process, we know each column in (3) must have a 0 value at some specific position after superimposing the adaptive DC bias. That means the generated CFMO-OFDM signal has $\frac{N}{2^L}$ inherent zeros. These inherent zero values may be distorted by the noise during transmission, thus resulting in a random offset from the zero value. Therefore, forcibly zeroing these values can reduce the noise of the corresponding carriers. After applying the period division operation to the received signal r_n according to (3), we have:

$$r\_M = \begin{bmatrix} r_{0+0\times\frac{N}{2^L}} & r_{1+0\times\frac{N}{2^L}} & \cdots & r_{\frac{N}{2^L}+0\times\frac{N}{2^L}-1} \\ r_{0+1\times\frac{N}{2^L}} & r_{1+1\times\frac{N}{2^L}} & \cdots & r_{\frac{N}{2^L}+1\times\frac{N}{2^L}-1} \\ \cdots & \cdots & \cdots & \cdots \\ r_{0+(2^L-1)\times\frac{N}{2^L}} & r_{1+(2^L-1)\times\frac{N}{2^L}} & \cdots & r_{\frac{N}{2^L}+(2^L-1)\times\frac{N}{2^L}-1} \end{bmatrix}. \tag{11}$$

Take the minimum value for each column of matrix r_M in (11), and this value will be considered as the original 0 value, and then force it to zero to achieve the effect of de-noising. This is the optimization process of the Re0 Rx. For the high signal-to-noise ratio (SNR), because the fluctuation degree of the signal is much greater than that of noise, the Re0 Rx shows good accuracy for the zero value, where theoretically, it can remove $\frac{1}{2^L}$ of the noise in the time domain. However, the period number increases with the layer number, thus resulting in the reduced number of inherent zeros and the performance gain in the Re0 Rx.

Next, the signal r_n is demodulated. Since there is no interlayer interference and DC bias effects on data subcarriers, a single FFT can be used to realize the time/frequency-domain conversion, which is given as:

$$R_K = \frac{1}{\sqrt{N}} \sum_{n=0}^{N-1} \tilde{r}_n \exp(-j\frac{2\pi}{N} kn). \tag{12}$$

The symbols on the corresponding frequency-domain carriers are recovered based on the maximum likelihood (ML) detection as given by:

$$\begin{aligned} \hat{X}_{2^{l-1}(2K+1)} = \underset{X\in\chi_{\mathrm{QAM}}}{\arg\min} \left\| X - R_{2^{l-1}(2K+1)} \right\|^2, \\ 0 \le K \le \tfrac{N}{2^{l+1}} \ 1 \le l \le L. \end{aligned} \tag{13}$$

where χ_{QAM} is the standard mapping set of QAM symbol.

III. Performance Analysis of CFMO-OFDM

In this section, the BER, SE, PAPR, and complexity of the proposed CFMO-OFDM scheme will be analyzed. In addition, comparisons of DCO-OFDM, HACO-OFDM, LACO-OFDM and the proposed scheme are given [30], [34].

A. BER analysis of CFMO-OFDM

The BER performance of CFMO-OFDM is analyzed under AWGN and its BER expression is provided in this part. For ACO-OFDM with a constellation size of M, the bit error probabilities can be formulated as [31]:

$$P_{b,\mathrm{QAM}} \approx \frac{4\left(\sqrt{M}-1\right)}{\sqrt{M}\log_2 M} Q\left(\sqrt{\frac{3}{M-1}\frac{E_s}{N_0}}\right), \tag{14}$$

where E_s denotes the electrical energy per subcarrier, N_0 represents noise power spectral density and $Q(.)$ is the tail probability of the standard normal distribution. Since all the subcarriers are modulated by the same modulation order (M) with equal power allocation in the proposed CFMO-OFDM, the branch BER performance of each layer should be the same

as:

$$P_{b,\mathrm{CFMO}(l)} = P_{b,\mathrm{QAM}} \approx \frac{4\left(\sqrt{M}-1\right)}{\sqrt{M}\log_2 M} Q\left(\sqrt{\frac{3}{M-1}\frac{E_s}{N_0}}\right). \tag{15}$$

From the angel of the weighted average of each layer, we can have the overall BER performance of the CFMO-OFDM system as:

$$P_{b,\mathrm{CFMO}} = \frac{\sum_{l=1}^{L} \frac{1}{2^{l+1}} \log_2 M \cdot P_{b,\mathrm{CFMO}(l)}}{\sum_{l=1}^{L} \frac{1}{2^{l+1}} \log_2 M} = P_{b,\mathrm{CFMO}(l)}, \tag{16}$$

which means the overall BER of CFMO-OFDM is also the same as the branch BER of each layer.

B. SE analysis of CFMO-OFDM

For the modulation order of M-QAM for each layer, the SE and the spectrum utilization (SU), in terms of M and L are given, respectively as:

$$\mathrm{SE}_{\mathrm{CFMO-OFDM}} = \frac{1}{2}\log_2 M - \frac{1}{2^{L+1}}\log_2 M \ (\mathrm{bit/s/Hz}). \tag{17}$$

It can be seen that the value of SE is determined by the order of QAM constellation and the number of layers. And from the perspective of spectrum utilization (SU), the SU of the proposed scheme can be expressed as:

$$\mathrm{SU}_{\mathrm{CFMO-OFDM}} = 1 - \frac{1}{2^L}. \tag{18}$$

Figure 4(a) depicts the plots for SU as a function of the number of layers for different schemes. As shown, the proposed scheme and LACO-OFDM have the same exponential profile reaching the saturated level of ~ 0.9 at $L = 6$, which is very close to 1 as in DCO-OFDM. For $L = 2$ the proposed scheme offers the same SU of 0.75 as HACO-OFDM. Also shown in Fig 4(b) is the SE of the proposed scheme as a function of M and L.

C. PAPR analysis of CFMO-OFDM

In real scenarios, the transmitted signal may suffer from the nonlinearities of the LEDs, amplifiers, and other archive devices, which can deteriorate the system's performance. Therefore, signals with lower PAPR are less susceptible to the nonlinearity in the system as well as relaxing the required dynamic ranges of A/D and D/A modules at the cost of increased BER. In this subsection, the complementary cumulative distribution function (CCDF) is used to compare the PAPR performance of the proposed scheme with other modulations for the same SE [46].

$$\mathrm{PAPR} = 10\log_{10}\frac{\max|x(n)|^2}{E\left[|x(n)|^2\right]} \quad (\mathrm{dB}). \tag{19}$$

In this part, all the subcarriers are modulated by the same modulation order (M) with equal power allocation, which is similar to Ref [21]. Take an OFDM system with limited total power P as an example, the power allocated to each subcarrier with the same M is equal to the mean power and can be calculated by P/N (N is the number of subcarriers) in the frequency domain. That means the power allocated to each subcarrier is only related to the number of subcarriers (i.e., N) and has nothing to do with the modulation order of M (no matter M = 4, 16, or 128). Since M is independent of the mean power, it will not influence the PAPR in this situation. Furthermore, from (19) we know that the peak power (i.e., the square of time-domain maximum amplitude) and the mean power (can also be calculated from the time domain) influence the PAPR. Since the maximum amplitude is generated by the in-phase superposition in multiple subcarrier modulation and the mean power can be calculated by P/N, the PAPR is mainly influenced by the number of subcarriers N in our simulation. Therefore, we set the number of subcarriers N as 512 to illustrate the PAPR performance of the proposed CFMO-OFDM for M of 16 and 64, and L of 2, 3, 4, and 5, as well as 3-layer, 16-QAM LACO-OFDM, 16-QAM, 8-PAM HACO-OFDM, and 128-QAM ACO-OFDM in Fig. 5. The coincident curves of M = 16 and 64 under the same L demonstrate the theoretical analysis of the proposed scheme. In addition, for $L \geq 2$, as the mean power of CFMO-OFDM signal increases with the layers, the PAPR decreases with more layers' utilization in CFMO-OFDM. This can also be verified from Fig. 5. Compared with LACO-OFDM, HACO-OFDM, and ACO-OFDM, the PAPR gains of CFMO-OFDM (i.e., CFMO-OFDM with L = 3 @ 16-QAM) are about 2.4, 3.2, and 4.4 dB at the $\Pr(\mathrm{PAPR} > \mathrm{PAPR}_0)$ of 10^{-4} with the same SE of 1.75 bit/s/Hz.

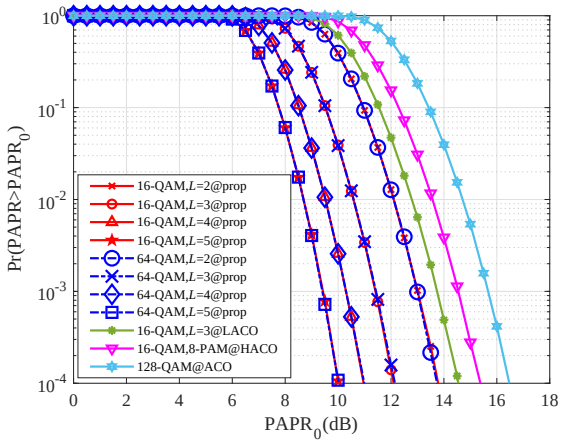

Fig. 5: PAPR performance curves of CFMO-OFDM scheme and other schemes ($N = 512$).

D. Complexity analysis of CFMO-OFDM

The system complexity is mainly due to the number of FFT/IFFT and ML operations during the process of signal generation and demodulation. In addition, CM, PC, and other optimization operations adopted in the proposed modulation schemes can enhance the complexity, but most of these signal processing are addition and subtraction and therefore are not significant and can be ignored compared to the FFT/IFFT

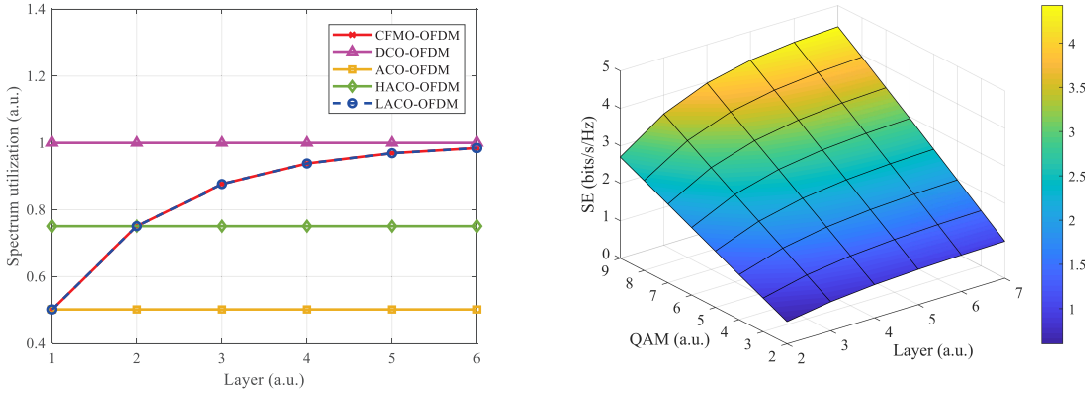

(a) SU of each scheme (b) SE of CFMO-OFDM

Fig. 4: Analysis of signal throughput capacity of each scheme.

operation. Note, for the same SE the complexity of ML operation for each system is almost similar, and therefore, we only focus on the complexity of the total FFT/IFFT operation at the transceiver.

The complexity of one-time N-point FFT/IFFT is expressed as $O(N\log_2 N)$ as adopted in [21]. The proposed scheme requires one-time N-point IFFT and FFT at the transmitter and Rx respectively, so the complexity of both the transmitter and receiver is $O(N\log_2 N)$. The complexity of the transceiver is similar to that of single-layer schemes such as ACO-OFDM and DCO-OFDM.

For the conventional L-layer LACO-OFDM scheme, the complexity of the Tx and the Rx can be expressed as:

$$\begin{aligned} O_{\mathrm{LACO}}^{\mathrm{tx}} &= \sum_{l=1}^{L} O(N/2^{l-1}\log_2(N/2^{l-1})) \\ &\approx (2-1/2^{L-1})O(N\log_2 N). \end{aligned} \tag{20}$$

$$\begin{aligned} O_{\mathrm{LACO}}^{\mathrm{rx}} &= O(N\log_2 N) + 2\sum_{l=1}^{L-1} O(N/2^{l-1}\log_2(N/2^{l-1})) \\ &\approx (5-1/2^{L-3})O(N\log_2 N). \end{aligned} \tag{21}$$

Considering the continuous improvement of the LACO-OFDM Rx in the presence of references [33] and [34], the realization of the Rx can be achieved by means of one N-point FFT operation with the complexity of $O(N\log_2 N)$, without affecting the Tx performance.

In the conventional HACO-OFDM, the Tx will require two N-point IFFT to realize signal generation, whereas for the signal recovery at the Rx two N-point FFT and one N-point IFFT are required. Therefore, the complexity of the Tx and the Rx can be expressed, respectively as:

$$O_{\mathrm{HACO}}^{\mathrm{tx}} = 2O(N\log_2 N). \tag{22}$$

$$O_{\mathrm{HACO}}^{\mathrm{rx}} = 3O(N\log_2 N). \tag{23}$$

In order to more intuitively observe the complexity of each system, table II contains the complexity caused by FFT / IFFT operation at the transceiver of the above systems, the complexity $O(N\log_2 N)$ is expressed in table II as O.

TABLE II: Complexity performance of different schemes.

Scheme	FFT/IFFT of Tx	FFT/IFFT of Rx
CFMO	O	O
DCO	O	O
ACO	O	O
LACO	$(2-\frac{1}{2^{L-1}})O$	$(5-\frac{1}{2^{L-3}})O$
LACO [34]	$(2-\frac{1}{2^{L-1}})O$	O
HACO	$2O$	$3O$

IV. Numerical Simulations and Experiments

In this section, the comprehensive numerical simulations including BER, coding algorithm, Re0 Rx, linear and nonlinear channel, and a proof-of-concept experiment are given and analyzed. The largest number of subcarriers among each layer in this section is still set to $N = 512$. A series of comparison cases are given in Table III. To be fair, each scheme of each case has the same SE.

A. Ideal linear channel

The BER performance plots against the E_b/N_0 for the proposed CFMO-OFDM with (w) and without (w/o) the Re0 Rx and forward error correction (FEC) code (i.e., the convolutional code (2, 1, 3) and (4, 3, [5 4 3])) under 16-QAM are shown in Fig. 6. As shown, at the BER of 10^{-4} and for L of 2, the Re0 Rx offers the E_b/N_0 gains of 1.1 dB for CFMO-OFDM, no matter with and without FEC. That means the BER performance can be enhanced by both the Re0 algorithm and FEC coding scheme. However, the BER improvement resulting from coded CFMO-OFDM is at the cost of reducing the transmission efficiency by half and a quarter, respectively. For a fair comparison, the uncoded OFDM schemes with the same SE are given in the following simulations. Also, from Fig. 6, we can see that the proposed scheme maintains consistent BER performance between the branch and total BER curves under the same modulation order of each layer, which is mainly

TABLE III: Simulation parameter setting.

	Scheme	Parameter
Case 1	CFMO	$L = 2$, 16-QAM
SE $= 1.5$ bit/s/Hz.	LACO	$L = 2$, 16-QAM
	LACO [34]	$L = 2$, 16-QAM
	HACO	16-QAM, 4-PAM
	DCO	8-QAM, $\beta = 6$ dB
Case 2	CFMO	$L = 3$, 16-QAM
SE $= 1.75$ bit/s/Hz.	LACO	$L = 3$, 16-QAM
	LACO [34]	$L = 3$, 16-QAM
	HACO	16-QAM, 8-PAM
	ACO	128-QAM
Case 3	CFMO	$L = 2$, 64-QAM
SE $= 2.25$ bit/s/Hz.	LACO	$L = 2$, 64-QAM
	LACO [34]	$L = 2$, 64-QAM
Case 4	CFMO	$L = 3$, 256-QAM
SE $= 3.5$ bit/s/Hz.	LACO	$L = 3$, 256-QAM
	LACO [34]	$L = 3$, 256-QAM
	HACO	512-QAM, 64-PAM
	DCO	128-QAM, $\beta = 9$ dB

because the proposed CFMO-OFDM system with equal power allocation does not suffer from the interlayer interference.

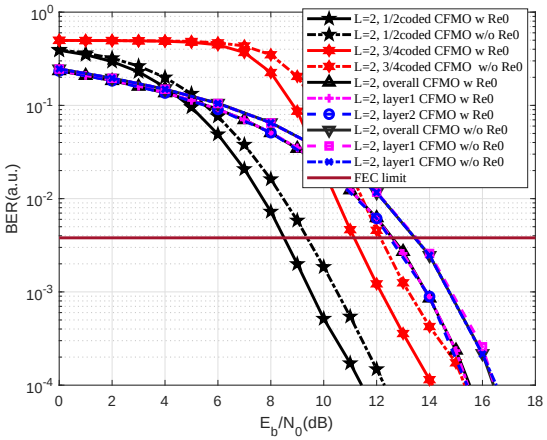

Fig. 6: BER performance curves of the proposed scheme with and without the Re0 Rx and convolution code (16QAM).

The performance comparison curve under case 1 is shown in Fig. 7(a), at the BER of 10^{-4} compared with (i) LACO-OFDM and improved LACO-OFDM reported in [34], CFMO-OFDM offers the E_b/N_0 gains of 0.8 and 0.5 dB, respectively; and (ii) HACO-OFDM, DCO-OFDM, and the proposed scheme show E_b/N_0 gains of 1, and 6.5 dB, respectively. In addition, the BER comparison under case 2 is shown in Fig. 7(b). As can be seen from Fig. 7(b), at higher E_b/N_0 the proposed scheme and LACO-OFDM have almost the same performance, whereas at lower E_b/N_0 the proposed scheme offers improved performance due to no interlayer-induced noise. E.g., at BER of 10^{-4}, which is lower than the FEC limit, the proposed scheme offers E_b/N_0 gains of 1.4, 2, and 4.6 dB compared with LACO-OFDM [34], HACO-OFDM, and ACO-OFDM, respectively. Note that, although the gain induced from Re0 Rx is decreasing with the increasing L, the BER gap between these OFDM schemes increases with the increasing L due to the presence or absence of interlayer interference. However, 2 and 3 layers of CFMO-OFDM show the best tradeoff between spectral efficiency and Re0 performance. Higher L ($L \geq 4$) attains only a tiny spectral efficiency gain, which is rarely used in real systems.

Without losing generality, Fig. 8 illustrates the comparison of BER performance plots for the SE of 2.25 and 3.5 bit/s/Hz under case 3 and case 4. Note, at the BER of 10^{-4} and for the SE of (i) 2.25 bit/s/Hz the proposed scheme attains 1, and 0.5 dB gains compared with LACO-OFDM, and LACO-OFDM [34], respectively, and (ii) 3.5 bit/s/Hz the proposed scheme offers the same and improved performance as LACO-OFDM at higher and lower E_b/N_0 values, respectively. Whereas, compared with LACO-OFDM [34], it shows a 1.1 dB gain, which is increased to 6.8 dB compared with HACO-OFDM. Note, for DCO-OFDM even 9 dB of DC bias still does not overcome the performance degradation induced by down clipping. Compared with the proposed scheme, the E_b/N_0 attenuation reaches about 6 dB at the BER of 10^{-4}.

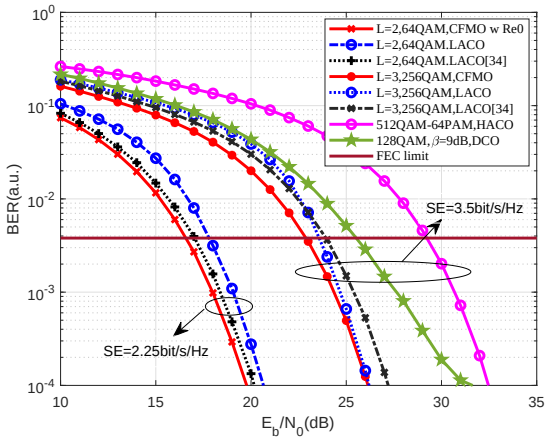

Fig. 8: Comparison of BER performance curves under different parameters for Case 3 and Case 4.

B. LED nonlinear channel

In a real scenario, the signal usually suffers from the nonlinear distortion of the LED Tx and other active devices. Therefore investigating the system performance for different modulation schemes considering the nonlinear distortion (in this case, the nonlinearity of the LED power-current characteristics) is also important. Here, the Rapper model is introduced to simulate LED nonlinearity, which is given by [47]:

$$I_n = \begin{cases} \frac{f(x_n)}{(1+(\frac{f(x_n)}{i_{\max}})^{2\lambda})^{\frac{1}{2\lambda}}}, & f(x_n) \geq 0, \\ 0, & f(x_n) < 0, \end{cases} \tag{24}$$

where I_n is the value obtained after nonlinear distortion, λ is the knee factor, which determines the smoothness of

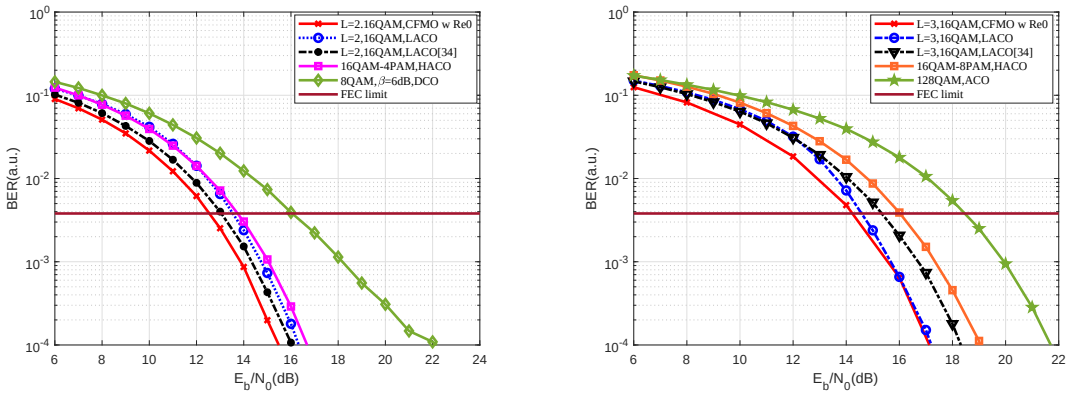

(a) (b)

Fig. 7: BER performance comparison between the proposed scheme and other schemes: (a) case 1, (b) case 2.

the nonlinear current-voltage characteristic curve, we define $f(x_n) = x_n/R$, and R is assumed to be a 1 Ω normalization resistance, $i_{\max}$ is the upper clipping limit, which is defined as:

$$\Phi = 10\log_{10}(\frac{i_{\max}^2}{\sigma^2}) \text{ dB}, \tag{25}$$

where Φ is the cutting factor, the smaller the value, the stricter the upper clipping limit. σ^2 is the electric power of the transmitted signal.

Figure 9 shows the BER performance plots as a function of E_b/N_0 for the proposed scheme as well as the other modulations for Case 1 and 2, and different LED nonlinear distortion degrees (i.e., λ and Φ). In Fig. 9(a) of case 1, all modulation schemes reach the SE of 1.5 bit/s/Hz under a large degree of nonlinear distortion (i.e., $\lambda = 3$, $\Phi = 8$ dB). However, in some schemes, the BER of 10^{-4}, which is just below the FEC BER limit, is not met. This is because the nonlinear distortion is the dominant source affecting the BER performance even in the case of a high E_b/N_0. However, the proposed scheme can achieve the BER of 10^{-4} at the E_b/N_0 of about 21 dB, and with a 3 dB gain compared with DCO-OFDM. From Fig. 9(b) of case 2, the SE is set to 1.75 bit/s/Hz for comparison. With the nonlinear distortion degree of $\lambda = 2$, and $\Phi = 10$ dB, we observed that all schemes except ACO-OFDM can reach the BER of 10^{-3} provided the upper clipping limit is not too stricter. Among these OFDM schemes, the proposed scheme still offers the best BER performance. This undoubtedly verifies the superior performance of the proposed scheme when considering the LED nonlinearity, which also confirms the PAPR analysis of the proposed scheme in part C of Section III.

Figure 10 depicts the BER plots of each system with the clipping coefficient for a specific E_b/N_0. At low values of Φ, the dominant limitation factor is the nonlinear distortion, whereas at higher values of Φ the degree of nonlinear distortion is very small and the dominant factor is AWGN. In Fig. 10(a), the simulation parameters are set to $\lambda = 3$ and E_b/N_0 of 15 dB for Case 1. We observe the BER performance of DCO-OFDM is superior to the other OFDM schemes for lower values of Φ. That is because DCO-OFDM with a bipolar signal has lower PAPR, which is non-susceptible to the nonlinear distortion. However, the communication system cannot work reliably under such BER. For higher values of Φ, the BER performance of DCO-OFDM are much worse than these advanced hybrid/layered modulation schemes. However, the proposed scheme shows improved BER performance compared to the other schemes. As shown in Fig. 10(b), the proposed scheme always shows the best performance under the same simulation conditions. At higher values of Φ, we note that (i) the BER performance is being dominated by the AWGN; and (ii) LACO-OFDM and CFMO-OFDM displaying almost the same BER performance for $\Phi > 14$dB, which is also consistent with the BER results shown in part A of Section IV for $L = 3$.

C. Proof-of-concept experiment and results

Finally, the proof-of-concept experiments are implemented to demonstrate the performance of proposed CFMO-OFDM system [48]. Figure 11(a) shows the experimental set-up, which mainly includes the arbitrary function generator (AFG, RIGOL DG 992), LED (Rebel Star 01), photodetector (PD, Thorlabs PDA36A), DC power supply (Keysight E36103A), and oscilloscope (OSC, Keysight DSOX1102G). The modulation and demodulation of each OFDM scheme are realized by MatLab 2019b via offline processing. In this experiment, the generated random signal with 2560 discrete samples is uploaded to the AFG with a modulation frequency of 2 MHz. Then, the output analog signal of AFG is coupled with a DC-bias current I_{dc} of about 220 mA to drive the LED at Tx. The PD output is directly connected to the OSC with a sampling frequency of 10 Msample/s. Under the same experimental distance of 70 cm, the proof-of-concept experiments of each OFDM scheme are repeated by 10 times to calculate the BER results as shown in Fig. 11(b). Limited by the maximum storage length of AFG, the BER results are not accurate enough compared with the numerical simulations ($> 1 \times 10^6$ iterations). Therefore, there are twice, once and zero times of no bit error exist respectively for CFMO-OFDM, LACO-OFDM and HACO-OFDM during the 10 times test. The mean

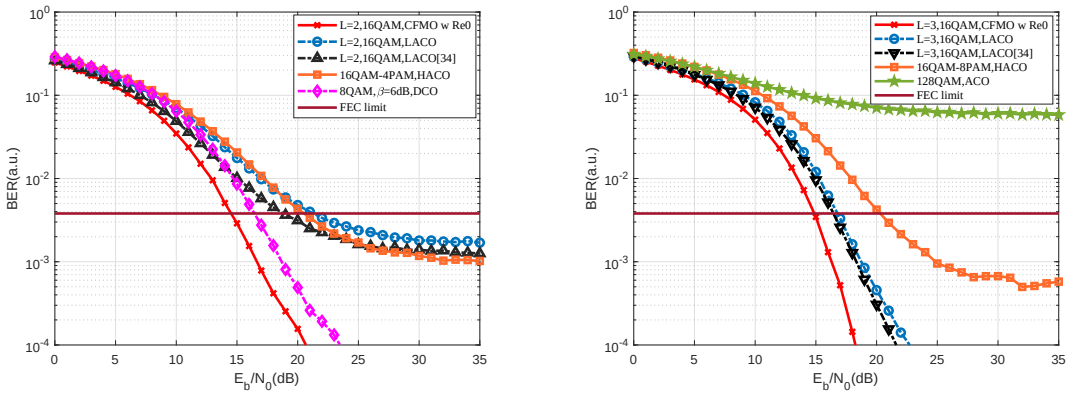

(a) (b)

Fig. 9: The BER performance versus the E_b/N_0 for the proposed and other modulation schemes with LED nonlinear channel: (a) $\lambda = 3$, $\Phi = 8$ dB for case 1, (b) $\lambda = 2$, $\Phi = 10$ dB for case 2.

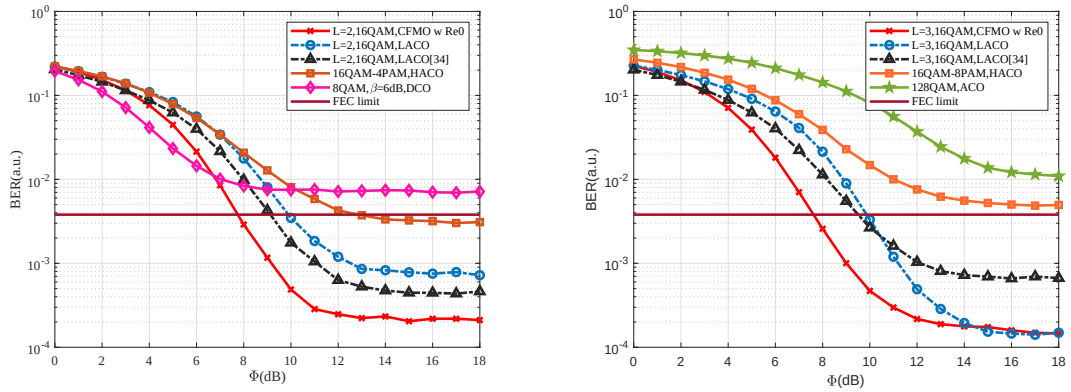

(a) (b)

Fig. 10: The plots for the BER versus the clipping factor Φ with E_b/N_0 of: (a) 15 dB, $\lambda = 3$ for Case 1, (b) 17 dB, $\lambda = 2$ for case 2.

BERs of CFMO-OFDM, LACO-OFDM and HACO-OFDM (set the same as case 1) are 5.125×10^{-4}, 5.685×10^{-4} and 5.732×10^{-4}, which are all below the FEC limit.

V. Conclusion

This paper proposed a low-complexity and high-performance CFMO-OFDM scheme for the IM/DD-based OWC system. At the Tx a clipping-free time-domain signal was first obtained by a single IFFT operation and thereafter superimposed with the periodic DC bias. Since the negative clipping operation was removed from the signal generation process there was no interlayer interference in the proposed system. In addition, at the Rx a single FFT was employed for demodulation with a novel Re0 Rx. Thus the proposed scheme offers advantages of both single-layer and hybrid/layered modulation schemes with reduced complexity and higher SE, respectively. However, there is an upper limit on the layer number since there is a tiny further improvement in the performance gain of the Re0 Rx beyond three layers of CFMO-OFDM. The simulation and experimental results show that the proposed scheme is superior to the state-of-the-art modulation schemes in spectral efficiency, bit error rate, and system complexity. Besides, due to the special signal synthesizing process, the proposed scheme shows a low peak-to-average power ratio, thus being non-susceptible to the nonlinearity of the light source and channel.

Acknowledgment

The authors would like to thank the anonymous reviewers for their precious time, valuable comments, and inspirational suggestions for improving this article.

References

[1] T. J. OShea, J. Hoydis, "An introduction to machine learning communications systems," *arXiv preprint arXiv:* 1702.00832, 2017.

[2] Z. Ghassemlooy, L. N. Alves, M-Ali Khalighi, "Visible Light Communications: Theory and Applications," *CRC Press.*, 2017

[3] L. E. M. Matheus, A. B. Vieira, L. F. M. Vieira, M. A. M. Vieira and O. Gnawali, "Visible Light Communication: Concepts, Applications and Challenges," *IEEE Communications Surveys & Tutorials*, vol. 21, no. 4, pp. 3204-3237, Fourth quarter 2019.

[4] Z. Ghassemlooy, S. Arnon, M. Uysal, Z. Xu and J. Cheng, "Emerging Optical Wireless Communications-Advances and Challenges," *IEEE Journal on Selected Areas in Communications*, vol. 33, no. 9, pp. 1738-1749, Sept. 2015.

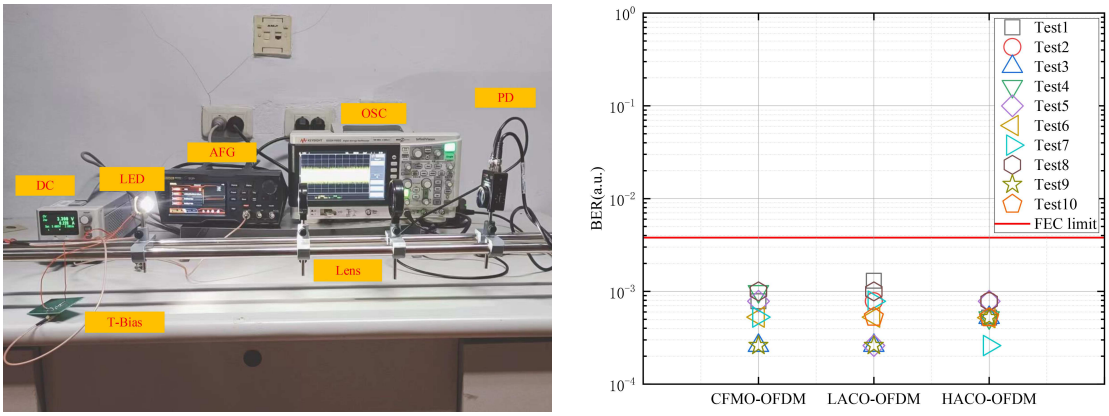

(a) (b)

Fig. 11: The proof-of-concept experiments: (a) the experimental set-up, (b) BER comparison for case 1.

[5] N. Chi, H. Haas, M. Kavehrad, T. D. C. Little and X. -L. Huang, "Visible light communications: demand factors, benefits and opportunities," *IEEE Wireless Communications*, vol. 22, no. 2, pp. 5-7, Apr. 2015.

[6] G. Pan, J. Ye and Z. Ding, "Secure Hybrid VLC-RF Systems With Light Energy Harvesting," *IEEE Transactions on Communications*, vol. 65, no. 10, pp. 4348-4359, Oct. 2017.

[7] X. Li, R. Zhang and L. Hanzo, "Cooperative Load Balancing in Hybrid Visible Light Communications and WiFi," *IEEE Transactions on Communications*, vol. 63, no. 4, pp. 1319-1329, Apr. 2015.

[8] J. M. Kahn and J. R. Barry, "Wireless infrared communications," *Proceedings of the IEEE*, vol. 85, no. 2, pp. 265-298, Feb. 1997.

[9] J. Gancarz, H. Elgala and T. D. C. Little, "Impact of lighting requirements on VLC systems," *IEEE Communications Magazine*, vol. 51, no. 12, pp. 34-41, Dec. 2013.

[10] G. Cossu, A. M. Khalid, P. Choudhury, R. Corsini, and E. Ciaramella, "3.4 Gbit/s visible optical wireless transmission based on RGB LED," *Optics Express* Vol. 20, pp. B501-B506, Dec. 2012.

[11] L. Cimini, "Analysis and Simulation of a Digital Mobile Channel Using Orthogonal Frequency Division Multiplexing," *IEEE Transactions on Communications*, vol. 33, no. 7, pp. 665-675, Jul. 1985.

[12] J. Armstrong, "OFDM for Optical Communications," *Journal of Lightwave Technology*, vol. 27, no. 3, pp. 189-204, Feb. 2009.

[13] O. Gonzalez, R. Perez-Jimenez, S. Rodriguez, et al., "Adaptive OFDM system for communications over the indoor wireless optical channel," *IEE Proceedings Optoelectronics*, vol. 153, no. 4, pp. 139-144, 2006.

[14] J. Armstrong, J. Lowery, "Power efficient optical OFDM," *Electronics Letters*, vol. 42, no. 6, pp. 370-372, Mar. 2006.

[15] S. C. J. Lee, S. Randel, F. Breyer and A. M. J. Koonen, "PAM-DMT for Intensity-Modulated and Direct-Detection Optical Communication Systems," *IEEE Photonics Technology Letters*, vol. 21, no. 23, pp. 1749-1751, Dec. 2009.

[16] R. Bai, Q. Wang and Z. Wang, "Asymmetrically Clipped Absolute Value Optical OFDM for Intensity-Modulated Direct-Detection Systems," *Journal of Lightwave Technology*, vol. 35, no. 17, pp. 3680-3691, Sept. 2017.

[17] S. D. Dissanayake, K. Panta and J. Armstrong, "A novel technique to simultaneously transmit ACO-OFDM and DCO-OFDM in IM/DD systems," *IEEE GLOBECOM Workshops*, 2011, pp. 782-786.

[18] T. Zhang, H. Ji, Z. Ghassemlooy, X. Tang, B. Lin and S. Qiao, "Spectrum-Efficient Triple-Layer Hybrid Optical OFDM for IM/DD-Based Optical Wireless Communications," *IEEE Access*, vol. 8, pp. 10352-10362, Jan. 2020.

[19] B. Li, X. Xue, S. Feng and W. Xu, "Layered Optical OFDM With Adaptive Bias for Dimming Compatible Visible Light Communications," *Journal of Lightwave Technology*, vol. 39, no. 11, pp. 3434-3444, Jun. 2021.

[20] B. Ranjha and M. Kavehrad, "Hybrid asymmetrically clipped OFDM-based IM/DD optical wireless system," *Journal of Optical Communications and Networking*, vol. 6, no. 4, pp. 387-396, Apr. 2014.

[21] Q. Wang, C. Qian, X. Guo, Z. Wang, D.G. Cunningham, I. H. White, "Layered ACO-OFDM for intensity-modulated direct-detection optical wireless transmission," *Optics Express*, vol. 23, no.9, pp. 12382-12393, May. 2015.

[22] Y. Sun, F. Yang and L. Cheng, "An Overview of OFDM-Based Visible Light Communication Systems From the Perspective of Energy Efficiency Versus Spectral Efficiency," *IEEE Access*, vol. 6, pp. 60824-60833, Oct. 2018.

[23] L. Deng, Y. Rui, P. Cheng, J. Zhang, Q. T. Zhang and M. Li, "A Unified Energy Efficiency and Spectral Efficiency Tradeoff Metric in Wireless Networks," *IEEE Communications Letters*, vol. 17, no. 1, pp. 55-58, Jan. 2013.

[24] C. Xiong, G. Y. Li, S. Zhang, Y. Chen and S. Xu, "Energy- and Spectral-Efficiency Tradeoff in Downlink OFDMA Networks," *IEEE Transactions on Wireless Communications*, vol. 10, no. 11, pp. 3874-3886, Nov. 2011.

[25] O. Amin, E. Bedeer, M. H. Ahmed and O. A. Dobre, "Energy EfficiencyCSpectral Efficiency Tradeoff: A Multiobjective Optimization Approach," *IEEE Transactions on Vehicular Technology*, vol. 65, no. 4, pp. 1975-1981, Apr. 2016.

[26] Q. Wang, Z. Wang and L. Dai, "Iterative Receiver for Hybrid Asymmetrically Clipped Optical OFDM," *Journal of Lightwave Technology*, vol. 32, no. 22, pp. 4471-4477, Nov. 2014.

[27] Q. Wang, Z. Wang, X. Guo and L. Dai, "Improved Receiver Design for Layered ACO-OFDM in Optical Wireless Communications," *IEEE Photonics Technology Letters*, vol. 28, no. 3, pp. 319-322, Feb. 2016.

[28] R. Bai, R. Jiang, T. Mao, et al., "Iterative receiver for ADO-OFDM with near-optimal optical power allocation," *Optics Communications*, vol. 387, pp. 350-356, Mar. 2017.

[29] T. Zhang, Y. Zou, J. Sun and S. Qiao, "Design of PAM-DMT-Based Hybrid Optical OFDM for Visible Light Communications," *IEEE Wireless Communications Letters*, vol. 8, no. 1, pp. 265-268, Feb. 2019.

[30] T. Wang, Y. Hou and M. Ma, "A Novel Receiver Design for HACO-OFDM by Time-Domain Clipping Noise Elimination," *IEEE Communications Letters*, vol. 22, no. 9, pp. 1862-1865, Sep. 2018.

[31] H. Ji, T. Zhang, S. Qiao and Z. Ghassemlooy, "Joint Dimming Control and Optimal Power Allocation for THO-OFDM Visible Light Communications," *IEEE Transactions on Communications*, vol. 69, no. 8, pp. 5352-5366, Aug. 2021.

[32] B. Li, S. Feng, W. Xu and Z. Li, "Interference-Free Hybrid Optical OFDM With Low-Complexity Receiver for Wireless Optical Communications," *IEEE Communications Letters*, vol. 23, no. 5, pp. 818-821, May. 2019.

[33] X. Liu, J. Li, J. Li and Z. Huang, "Analysis of the Single-FFT Receiver for Layered ACO-OFDM in Visible Light Communications," *Journal of Lightwave Technology*, vol. 38, no. 17, pp. 4757-4764, Sept. 2020.

[34] J. Li, X. Liu, Y. Ren and Z. Huang, "Single-FFT Receiver With Pairwise Maximum Likelihood for Layered ACO-OFDM," *IEEE Photonics Journal*, vol. 13, no. 4, pp. 1-6, Aug. 2021.

[35] Y. Sun, F. Yang and J. Gao, "Comparison of Hybrid Optical Modulation Schemes for Visible Light Communication," *IEEE Photonics Journal*, vol. 9, no. 3, pp. 1-13, Jun. 2017.

[36] A. J. Lowery, "Spectrally efficient optical orthogonal frequency division multiplexing," *Philosophical Transactions of the Royal Society A*, vol. 378, p. 20190180, Mar. 2020.

[37] F. Yang, Y. Sun and J. Gao, "Adaptive LACO-OFDM With Variable Layer for Visible Light Communication," *IEEE Photonics Journal*, vol. 9, no. 6, pp. 1-8, Dec. 2017.

[38] A. Weiss, A. Yeredor and M. Shtaif, "Iterative Symbol Recovery for Power-Efficient DC-Biased Optical OFDM Systems," *Journal of Lightwave Technology*, vol. 34, no. 9, pp. 2331-2338, May. 2016.
[39] S. D. Dissanayake and J. Armstrong, "Comparison of ACO-OFDM, DCO-OFDM and ADO-OFDM in IM/DD Systems," *Journal of Lightwave Technology*, vol. 31, no. 7, pp. 1063-1072, Apr. 2013.
[40] T. Q. Wang, H. Li and X. Huang, "Analysis and Mitigation of Clipping Noise in Layered ACO-OFDM Based Visible Light Communication Systems," *IEEE Transactions on Communications*, vol. 67, no. 1, pp. 564-577, Jan. 2019.
[41] T. Zhang, Y. Zou, J. Sun and S. Qiao, "Improved Companding Transform for PAPR Reduction in ACO-OFDM-Based VLC Systems," *IEEE Communications Letters*, vol. 22, no. 6, pp. 1180-1183, Jun. 2018.
[42] J. Wang, Y. Xu, X. Ling, R. Zhang, Z. Ding, and C. Zhao, "PAPR analysis for OFDM visible light communication," *Optics Express*, vol. 24, pp. 27457-27474, Nov. 2016.
[43] J. Armstrong, B. J. .C Schmidt, D. Kalra, et al. "SPC07-4: Performance of asymmetrically clipped optical OFDM in AWGN for an intensity modulated direct detection system," *IEEE Globecom* 2006, pp. 1-5.
[44] X. Li, R. Mardling and J. Armstrong, "Channel capacity of IM/DD optical communication system and of ACO-OFDM," *IEEE International Conference on Communications*, 2007.
[45] J. Armstrong, B.J.C. Schmidt, "Comparison of asymmetrically clipped optical OFDM and DC-biased optical OFDM in AWGN," *IEEE Communications Letters*, vol. 12, no. 5, pp. 343C345, May. 2008.
[46] X. Wang, T. T. Tjhung and C. S. Ng, "Reduction of peak-to-average power ratio of OFDM system using a companding technique," *IEEE Transactions on Broadcasting*, vol. 45, no. 3, pp. 303-307, Sep. 1999.
[47] H. Elgala, R. Mesleh and H. Haas, "An LED Model for Intensity-Modulated Optical Communication Systems," *IEEE Photonics Technology Letters*, vol. 22, no. 11, pp. 835-837, Jun. 2010.
[48] T. Zhang, Z. Ghassemlooy, S. Rajbhandari, W. O. Popoola, S. X. Guo,"OFDM-PWM scheme for visible light communications," *Optics Communications*, vol. 385, pp. 213-218, Nov. 2016.

HONGXU WANG received the B.Sc. degree in Engineering from Changchun University of Technology, Changchun, China, in 2019. He is currently pursuing his master's degree in Control science and Engineering from School of Physics, Northeast Normal University, Changchun, China. His current research interests include the BER improvement, spectral efficiency enhancement and dimming control for visible light communications.

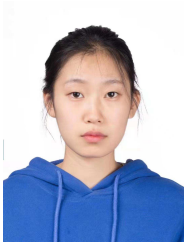

HUIXIN ZHANG received the B.Sc. degree in Engineering from Yantai University, Yantai, China, in 2020. She is currently pursuing her master's degree in Electronic information from School of Physics, Northeast Normal University, Changchun, China. Her current research interests include the PAPR reduction, spectral efficiency enhancement and dimming control for visible light communications.

ZABIH GHASSEMLOOY (Senior Member, IEEE) received the B.Sc. (Hons.) degree in electrical and electronics engineering from Manchester Metropolitan University, U.K., in 1981, and the M.Sc. and Ph.D. degrees from the University of Manchester, U.K., in 1984 and 1987, respectively. From 1987 to 1988, he was a Postdoctoral Research Fellow with the City, University of London, U.K. In 1988, he joined Sheffield Hallam University as a Lecturer, where he became a Professor, in 1997. In 2004, he joined the University of Northumbria, Newcastle upon Tyne, as the Associate Dean (AD) of research with the School of Engineering. From 2012 to 2014, he was the AD of the Research and Innovation, Faculty of Engineering and Environment, where he is currently the Head of the Optical Communications Research Group. He was a Research Fellow and a Distinguished Professor with the Chinese Academy of Science, Quanzhou, China, in 2015 and 2016, respectively. He was a Visiting Professor with University Tun Hussein Onn Malaysia, from 2013 to 2017, and Huaqiao University, China, from 2017 to 2018. He has published over 850 articles (330 journals and eight books), 97 keynote/invited talks, and supervised 65 Ph.D. students. He is also a coauthor of a CRC book on Optical Wireless Communications Systems and Channel Modeling with Matlab (First Edition 2012 and Second Edition 2019). His research interests include optical wireless communications, free space optics, visible light communications, radio over fibre-free space optics, and sensor networks with project funding from EU, U.K. Research Council and industry. He is also a Fellow of IET and OSA. He was the Vice-Chair of EU Cost Action IC1101, from 2011 to 2016. In 2001, he was awarded the Tan Chin Tuan Fellowship in engineering from Nanyang Technological University, Singapore. He has been the Vice-Chair of the OSA Technical Group of Optics in Digital Systems, since 2018. He is also the Founder and the Chair of the IEEE/IET International Symposium on Communications Systems, Networks and DSP and West Asian Colloquium on Optical Wireless Communications. He has been the Co-Founder of a number of international events, including Workshop on Optical Wireless Communications in ICC, since 2015. He has been the Chair of the IEEE Student Branch at Northumbria University, Newcastle upon Tyne, since 2019. From 2004 to 2006, he was the IEEE U.K./IR Communications Chapter Secretary, the Vice-Chairman, from 2006 to 2008, the Chairman, from 2008 to 2011, and the Chairman of the IET Northumbria Network from, October 2011 to 2015.

TIAN ZHANG received the B.Sc. and the M.Sc. degrees in electronic science and technology from the Changchun University of Science and Technology, Changchun, China, in 2010 and 2013, respectively, and the Ph.D. degree in electronic circuit and systems from State Key Laboratory of Integrated Optoelectronics, College of Electronic Science and Engineering, Jilin University, Changchun, in 2017. From 2015 to 2016, he was a visiting Ph.D. student with the Optical Communication Research Group (OCRG), University of Northumbria, Newcastle upon Tyne, U.K. He was a Lecturer and associate professor with the School of Physics, Northeast Normal University, Changchun, in 2017 and 2021. He has authored over twenty IEEE, OSA, IET, Elsevier journals, and seven conference papers. His current research interests include optical wireless communications and digital image processing.